Chapter 1

Nuclear Fusion II

> *"The fusion rate is $n_1 n_2 \langle \sigma v \rangle$: density squared times a thermal average that hides the Gamow peak."*
>
> standard plasma-nuclear summary [6, 14]

Lecture 25 introduced fusion energetics and the Coulomb barrier. This chapter derives the reaction rate from first principles (beam–target and plasma), derives the standard low-energy S-factor form, forms the thermal average, and identifies the Gamow peak that dominates thermonuclear burning. The discussion closes with the practical preference for D+T in laboratory fusion [6, 1, 14, 2].

1.1 Reaction rate from flux and cross section

1.1.1 Beam on a fixed target

Consider a beam of nuclei Y with number density n_Y and speed v incident on a target containing nuclei X. The fusion (or reaction) cross section σ is an effective area: if a Y trajectory would pierce the area σ centred on an X, a reaction occurs with the probability built into the definition of σ.

In a time $\mathrm{d}t$, each X is exposed to all Y particles that lie in a cylinder of base area σ and length $v\,\mathrm{d}t$. The volume of that cylinder is $\sigma v\,\mathrm{d}t$, so the number of Y nuclei in it is

$$n_Y\,\sigma\,v\,\mathrm{d}t. \tag{1.1}$$

The reaction rate *per target nucleus* X is therefore

$$\lambda_X = n_Y\,\sigma\,v. \tag{1.2}$$

If the number density of X is n_X, the number of reactions per unit volume per unit time is

$$R = n_X\,n_Y\,\sigma\,v. \tag{1.3}$$

This is the fundamental connection between microscopic cross section and macroscopic rate.

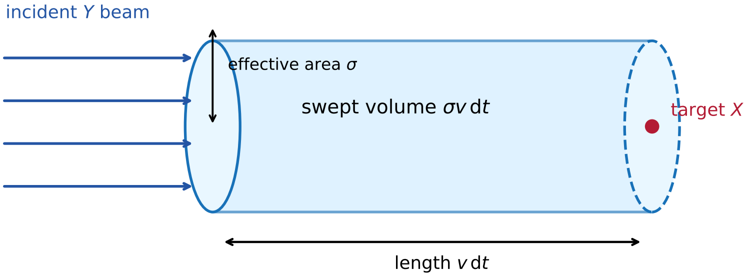

Figure 1.1: Vector redraw of the swept-volume construction. In time $\mathrm{d}t$, the effective reaction area σ sweeps the relative volume $\sigma v\,\mathrm{d}t$ past one target nucleus.

1.1.2 Thermonuclear plasma

In a fusion plasma both species move randomly; there is no laboratory "beam" and no fixed target. The same geometry applies in the *relative* frame: for any chosen X, construct the cylinder using the relative velocity v of approaching Y nuclei. Averaging over the thermal distribution of relative velocities replaces σv by its mean:

$$\boxed{r_{XY} = \frac{n_X n_Y}{1+\delta_{XY}}\,\langle\sigma v\rangle.} \tag{1.4}$$

For $X \neq Y$, there are $N_X N_Y$ unlike pairs in a volume. For $X = Y$, the number of unordered pairs is $N_X(N_X-1)/2 \simeq N_X^2/2$, not N_X^2; this proves the $1/(1+\delta_{XY})$ factor and identifies the double counting it removes. Once a fusion event occurs the participating nuclei are consumed; the instantaneous rate law is unchanged because the densities evolve in time.

The dimensions provide a useful check:

$$[n_X n_Y\langle\sigma v\rangle] = \mathrm{m}^{-6}\,(\mathrm{m}^2)(\mathrm{m\,s}^{-1}) = \mathrm{m}^{-3}\,\mathrm{s}^{-1}, \tag{1.5}$$

exactly reactions per unit volume per unit time. The reactivity $\langle\sigma v\rangle$ has SI units $\mathrm{m}^3\,\mathrm{s}^{-1}$ [6, 1, 14].

Key idea

Beam–target: $r = n_X n_Y \sigma v$ from the cylinder volume $\sigma v\,\mathrm{d}t$. Plasma: $r_{XY} = n_X n_Y\langle\sigma v\rangle/(1+\delta_{XY})$.

1.2 Thermal averaging of the fusion reactivity

For each Cartesian component, thermal velocities of the two species are independent Gaussians,

$$f_i(v_{i,x}) = \left(\frac{m_i}{2\pi k_B T}\right)^{1/2}\exp\left(-\frac{m_i v_{i,x}^2}{2k_B T}\right). \tag{1.6}$$

The relative component $v_x = v_{1,x} - v_{2,x}$ is therefore Gaussian with variance

$$\langle v_x^2\rangle = k_B T\left(\frac{1}{m_1}+\frac{1}{m_2}\right) = \frac{k_B T}{\mu}, \qquad \frac{1}{\mu} = \frac{1}{m_1}+\frac{1}{m_2}. \tag{1.7}$$

Multiplying the three component distributions gives the isotropic relative-velocity density

$$F(\boldsymbol{v}) = \left(\frac{\mu}{2\pi k_B T}\right)^{3/2} \exp\left(-\frac{\mu v^2}{2k_B T}\right), \qquad \int F(\boldsymbol{v})\,\mathrm{d}^3 v = 1. \tag{1.8}$$

Integrating over solid angle, $\mathrm{d}^3 v = 4\pi v^2 \mathrm{d}v$, yields the Maxwell–Boltzmann *relative-speed* distribution

$$f(v)\,\mathrm{d}v = 4\pi v^2 \left(\frac{\mu}{2\pi k_B T}\right)^{3/2} \exp\left(-\frac{\mu v^2}{2k_B T}\right) \mathrm{d}v. \tag{1.9}$$

It is μ, not either individual mass, that must appear. Writing $f(v)\,\mathrm{d}v$ for the probability that the relative speed lies in $[v, v + \mathrm{d}v]$,

$$\langle \sigma v \rangle = \int_0^\infty \sigma(v)\, v\, f(v)\,\mathrm{d}v. \tag{1.10}$$

To change variables to relative kinetic energy,

$$E = \frac{1}{2}\mu v^2, \qquad v\,\mathrm{d}v = \frac{\mathrm{d}E}{\mu}, \qquad v^2 = \frac{2E}{\mu}. \tag{1.11}$$

The Maxwellian speed weight contains $v^2 \exp(-\mu v^2/2k_B T)\,\mathrm{d}v$. Rewrite

$$v^2\,\mathrm{d}v = v\,(v\,\mathrm{d}v) = \sqrt{\frac{2E}{\mu}}\,\frac{\mathrm{d}E}{\mu} = \frac{\sqrt{2}}{\mu^{3/2}}\,E^{1/2}\,\mathrm{d}E,$$

or equivalently, combining with the extra factor of v in $\sigma(v)\,v$,

$$v^3\,\mathrm{d}v = v^2\,(v\,\mathrm{d}v) = \frac{2E}{\mu}\cdot\frac{\mathrm{d}E}{\mu} = \frac{2E\,\mathrm{d}E}{\mu^2}.$$

Inserting the normalized relative Maxwellian into Eq. (1.10) and collecting constants yields

$$\langle \sigma v \rangle = \left(\frac{8}{\pi\mu}\right)^{1/2} \frac{1}{(k_B T)^{3/2}} \int_0^\infty \sigma(E)\,E\,e^{-E/k_B T}\,\mathrm{d}E. \tag{1.12}$$

The dimensions are $(\mathrm{kg}^{-1/2}\mathrm{J}^{-3/2})(\mathrm{m}^2\,\mathrm{J}^2) = \mathrm{m}^3\,\mathrm{s}^{-1}$, as required.

1.3 Low-energy fusion cross section

Two ingredients dominate $\sigma(v)$ at thermonuclear energies ($E \sim \mathrm{keV} \ll V_{\mathrm{max}}$):

1.3.1 Barrier penetration

For two charges, define the Sommerfeld parameter

$$\eta(E) = \frac{Z_1 Z_2 e^2}{4\pi\varepsilon_0 \hbar v} = Z_1 Z_2 \alpha \sqrt{\frac{\mu c^2}{2E}}. \tag{1.13}$$

The Coulomb penetrability is

$$P_{\text{pen}} \propto e^{-2\pi\eta} = \exp\left[-\sqrt{\frac{E_G}{E}}\right], \qquad E_G = 2\mu c^2(\pi\alpha Z_1 Z_2)^2. \tag{1.14}$$

There is no convention-dependent factor left: the full exponent is $2\pi\eta = \sqrt{E_G/E}$. In practical units,

$$E_G = 0.978\, Z_1^2 Z_2^2 \mu_{\text{u}}\, \text{MeV}, \qquad 2\pi\eta = 31.29\, Z_1 Z_2 \sqrt{\frac{\mu_{\text{u}}}{E_{\text{keV}}}}, \tag{1.15}$$

where μ_{u} is the reduced mass in atomic mass units and E_{keV} is the centre-of-mass energy in keV.

1.3.2 Geometrical and quantum low-energy factor

The original lecture motivates the entrance-channel factor through impact parameters. At low energy the reduced de Broglie wavelength $\bar{\lambda} = \hbar/(\mu v) = 1/k$ can be large compared with the nuclear radius R. Quantise the orbital angular momentum semiclassically, $L \simeq \mu v b = (\ell + \frac{1}{2})\hbar$. The exact partial-wave reaction cross section has the structure

$$\sigma_{\text{r}}(E) = \frac{\pi}{k^2}\sum_{\ell=0}^{\infty}(2\ell+1)T_\ell(E), \qquad k = \frac{\sqrt{2\mu E}}{\hbar}, \tag{1.16}$$

where $0 \le T_\ell \le 1$ is a transmission coefficient. Thus each partial-wave prefactor carries $\pi/k^2 \propto 1/E \propto 1/v^2$, but T_ℓ contains the dominant Coulomb penetrability and nuclear dynamics; the prefactor alone is not the fusion cross section. The slide's annular construction recovers the same scaling: Quantise the impact parameter by angular momentum $L = \ell\hbar = \mu v b_\ell$, so

$$b_\ell = \frac{\ell\hbar}{\mu v}. \tag{1.17}$$

The annular area between ℓ and $\ell + 1$ is

$$A_\ell = \pi b_{\ell+1}^2 - \pi b_\ell^2 = \frac{\pi\hbar^2}{\mu^2 v^2}(2\ell+1). \tag{1.18}$$

Summing sharp-cutoff annuli to $\ell_{\max} \approx \mu v R/\hbar$ gives the heuristic geometric estimate

$$\sigma_{\text{geom}} \sim \pi\Big(R + \frac{\hbar}{\mu v}\Big)^2. \tag{1.19}$$

At sufficiently low energy the s-wave often dominates. For a *nonresonant binary charged-particle reaction*, it is useful to factor the cross section into a kinematic $1/E$, Coulomb penetration, and residual nuclear factor. This does not imply that the observable cross section itself rises as $1/E$, because the exponential suppression overwhelms that prefactor as $E \to 0$.

1.3.3 Combined low-energy form

The standard nuclear-astrophysics parametrisation for such a reaction is

$$\boxed{\sigma(E) = \frac{S(E)}{E}\,\exp\left[-\sqrt{\frac{E_G}{E}}\right]}\,. \tag{1.20}$$

where $S(E)$ is the slowly varying **astrophysical S-factor** and $[S] = [\sigma E]$, commonly keV b. This form applies to nonresonant binary charged-particle reactions away from thresholds. A resonance can make $S(E)$ vary rapidly, and then a Breit–Wigner or multichannel treatment must replace the "slowly varying S" approximation [6, 14, 1].

Remark

The raw lecture's statement that a large de Broglie wavelength by itself "increases" the fusion cross section is incomplete: the transmission coefficient contains the overwhelming factor $e^{-2\pi\eta}$. The standard $S(E)/E$ factorization keeps the kinematic $1/E$ and the Coulomb suppression separate.

1.4 The Gamow peak

Insert Eq. (1.20) into Eq. (1.12). The factor E in the Maxwellian integral cancels the $1/E$ in σ:

$$\langle \sigma v\rangle = \left(\frac{8}{\pi\mu}\right)^{1/2}\frac{1}{(k_BT)^{3/2}}\int_0^\infty S(E)e^{-\Phi(E)}\,\mathrm{d}E, \quad \Phi(E) = \frac{E}{k_BT} + \sqrt{\frac{E_G}{E}}. \tag{1.21}$$

The first term in Φ penalizes the rare high-energy Maxwell tail; the second penalizes low-energy Coulomb penetration. For a slowly varying $S(E)$, the maximum of the integrand is the minimum of Φ. Every calculus step is

- Differentiate:
$$\Phi'(E) = \frac{1}{k_BT} - \frac{1}{2}\sqrt{E_G}\,E^{-3/2}.$$
- Set $\Phi'(E_0) = 0$:
$$\frac{1}{k_BT} = \frac{\sqrt{E_G}}{2E_0^{3/2}} \implies E_0^{3/2} = \frac{\sqrt{E_G}\,k_BT}{2}.$$
- Raise both sides to 2/3:
$$\boxed{E_0 = \left[\frac{E_G(k_BT)^2}{4}\right]^{1/3}}. \tag{1.22}$$

At the stationary point, $\sqrt{E_G/E_0} = 2E_0/(k_BT)$, hence

$$\Phi(E_0) = \frac{3E_0}{k_BT}. \tag{1.23}$$

To obtain the width, differentiate again and use the stationary-point condition:

$$\Phi''(E) = \frac{3}{4}\sqrt{E_G}E^{-5/2}, \qquad \Phi''(E_0) = \frac{3}{2E_0 k_B T}. \tag{1.24}$$

Taylor expansion through second order gives

$$e^{-\Phi(E)} \simeq e^{-3E_0/k_B T} \exp\left[-\frac{3(E-E_0)^2}{4E_0 k_B T}\right]. \tag{1.25}$$

Define Δ as the full width between points where this Gaussian is $1/e$ of its maximum. Setting $E - E_0 = \pm\Delta/2$ gives

$$\frac{3(\Delta/2)^2}{4E_0 k_B T} = 1 \quad \Longrightarrow \quad \boxed{\Delta = 4\sqrt{\frac{E_0 k_B T}{3}}}. \tag{1.26}$$

Thus the effective nonresonant window is approximately $E_0 - \Delta/2 < E < E_0 + \Delta/2$. With $T_9 = T/(10^9\,\mathrm{K})$, $\mu_\mathrm{u} = \mu/\mathrm{u}$, and energies in MeV,

$$E_0 = 0.1220\left(Z_1^2 Z_2^2 \mu_\mathrm{u} T_9^2\right)^{1/3}\ \mathrm{MeV}, \tag{1.27}$$

$$\Delta = 0.2368\left(Z_1^2 Z_2^2 \mu_\mathrm{u}\right)^{1/6} T_9^{5/6}\ \mathrm{MeV}. \tag{1.28}$$

These constants use $\alpha = 1/137.036$, $1\,\mathrm{u}\,c^2 = 931.494\,\mathrm{MeV}$, and $k_B = 8.61733\times10^{-11}\,\mathrm{MeV\,K^{-1}}$.

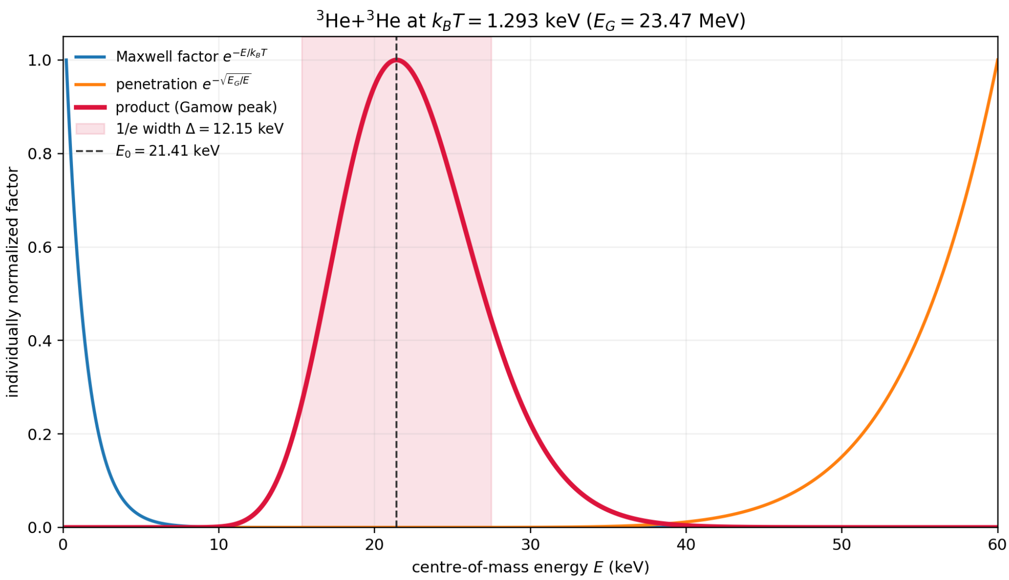

Figure 1.2: Maxwell factor, Coulomb penetration, and their product for $^3\mathrm{He} + {}^3\mathrm{He}$ at $k_BT = 1.293\,\mathrm{keV}$. With $Z_1Z_2 = 4$ and $\mu \simeq 1.50\,\mathrm{u}$, $E_G = 23.47\,\mathrm{MeV}$, $E_0 = 21.40\,\mathrm{keV}$, and the full $1/e$ width is $\Delta \simeq 12.15\,\mathrm{keV}$. Curves are individually normalized to show their competing energy dependence.

If $S(E) \simeq S(E_0)$, the Gaussian integral also yields the useful steepest-descent estimate

$$\langle\sigma v\rangle \simeq \left(\frac{32E_0}{3\mu}\right)^{1/2} \frac{S(E_0)}{k_B T} \exp\left(-\frac{3E_0}{k_B T}\right). \tag{1.29}$$

Key idea

Gamow peak: $E_0 = [E_G(k_BT)^2/4]^{1/3}$, $\Delta = 4\sqrt{E_0 k_B T/3}$, and $\Phi(E_0) = 3E_0/(k_BT)$. Fusion rates are exponentially temperature sensitive through this window.

The saddle-point formulas above assume a binary, nonresonant reaction with $S(E)$ nearly constant across the window. If a narrow resonance lies in or near that window, the rate is controlled by the resonance energy and strength rather than by $S(E_0)$. The D–T reaction is strongly enhanced by a broad compound-nuclear resonance, so fitted or evaluated reactivities are used for quantitative reactor calculations. The triple-alpha process is outside the binary formula altogether: it proceeds sequentially through the short-lived ^{8}Be system and the Hoyle-state resonance in ^{12}C [1, 14].

As temperature increases, E_0 shifts upward, the peak height grows rapidly, and $\langle\sigma v\rangle$ rises by many orders of magnitude. At extremely high T the simple low-energy form of σ eventually fails and other physics (resonances, different partial waves) enters; for solar and most laboratory fusion discussions the Gamow picture is the right first tool [14, 6, 2].

1.5 Putting it together: plasma reactivity

The volumetric reaction rate and locally deposited power density are

$$r_{XY} = \frac{n_X n_Y}{1+\delta_{XY}}\langle\sigma v\rangle(T), \tag{1.30}$$

$$p_{\rm dep} = r_{XY}\, Q_{\rm dep}. \tag{1.31}$$

Here $Q_{\rm dep} = Q - \langle E_\nu\rangle - \cdots$ excludes energy carried away by weakly interacting particles or other escaping products; in a blanket, escaping fusion neutrons can instead be recovered as heat. The Salpeter factor introduced in Lecture 25 applies only in the weak-screening, Debye–Hückel limit

$$\epsilon_{\rm sc} \equiv \frac{Z_1 Z_2 e^2}{4\pi\varepsilon_0 R_D k_B T} \ll 1, \qquad N_D \equiv \frac{4\pi}{3} R_D^3 \sum_s n_s \gg 1. \tag{1.32}$$

The first condition says that the screening free-energy correction is small compared with k_BT; the second ensures that a Debye sphere contains many particles. Strongly coupled or degenerate plasmas require a different screening treatment [36]. Design of a fusion reactor therefore requires:

(i) high density product $n_X n_Y$ (or n^2 for a single species);

(ii) high temperature so that $\langle\sigma v\rangle$ is appreciable;

(iii) sufficient confinement time for the plasma to react before cooling or disassembling (Lawson criterion: $n\tau_E$ above a threshold depending on T and the fuel cycle).

1.5.1 Why deuterium–tritium fuel?

Among light-ion reactions, deuterium–tritium fusion

$$^2\text{H} + {}^3\text{H} \;\to\; {}^4\text{He} + n + 17.6\,\text{MeV} \tag{1.33}$$

has the largest $\langle\sigma v\rangle$ at the lowest temperature of any practical fuel cycle: $Z_1 Z_2 = 1$ (same as *pp* or DD) but a more favourable nuclear matrix element and a broad ^{5}He compound-nuclear resonance. Consequently, the slowly varying-S Gamow approximation explains the Coulomb trend but is not a precision model of the D–T reactivity. Coulomb barriers for $\mathrm{D} + {}^3\mathrm{He}$ or pure proton fuels are higher or the weak interaction intervenes (*pp*), making them harder for terrestrial reactors. Stellar cores burn hydrogen via the slow *pp* chain precisely because weak interactions set the pace; stars have billions of years [6, 1, 14]. The rare solar hep branch,

$$ {}^3\mathrm{He} + p \to {}^4\mathrm{He} + e^+ + \nu_e, \tag{1.34} $$

produces the highest-energy standard solar neutrinos, with endpoint $E_\nu \simeq 18.77\,\mathrm{MeV}$, although its flux is tiny [36]. Two-body momentum conservation divides the 17.6 MeV into about 3.5 MeV for the α and 14.1 MeV for the neutron. Deuterium alone can burn through

$$ \mathrm{D} + \mathrm{D} \to \mathrm{T} + p + 4.03\,\mathrm{MeV}, \tag{1.35} $$
$$ \mathrm{D} + \mathrm{D} \to {}^3\mathrm{He} + n + 3.27\,\mathrm{MeV}, \tag{1.36} $$

with comparable low-energy branches, but substantially lower reactivity than D–T at reactor temperatures [1].

Caution

High T alone is not enough: without density and confinement, a hot plasma radiates and expands before fusing. The triple product $nT\tau_E$ is the usual figure of merit for ignition studies.

1.6 Summary of the fusion rate theory

Collecting the chain of reasoning:

(1) Geometry: each X sweeps a volume $\sigma v\,\mathrm{d}t$ relative to the Y gas; unordered-pair counting gives $r_{XY} = n_X n_Y \langle\sigma v\rangle/(1+\delta_{XY})$.

(2) Thermal average: replace σv by $\langle\sigma v\rangle = \int \sigma(v) v f(v)\,\mathrm{d}v$.

(3) Nonresonant binary charged-particle cross section: $\sigma = S(E)E^{-1}e^{-\sqrt{E_G/E}}$; resonances require their own energy-dependent treatment.

(4) Maxwell $\times$ Gamow $\Rightarrow$ Gamow peak at $E_0 \propto T^{2/3}$.

(5) Deposited power density $p_{\mathrm{dep}} = r_{XY} Q_{\mathrm{dep}}$; $\mathrm{D} + \mathrm{T}$ maximises reactivity for laboratory T.

Takeaway

- $r_{XY} = n_X n_Y \langle\sigma v\rangle/(1+\delta_{XY})$, with units $\mathrm{m}^{-3}\,\mathrm{s}^{-1}$.
- $\langle\sigma v\rangle = \int \sigma(v) v f(v)\,\mathrm{d}v$ (Maxwellian).
- Barrier penetration $e^{-2\pi\eta} = e^{-\sqrt{E_G/E}}$.

- For nonresonant binary charged-particle reactions, $\sigma(E) = S(E)E^{-1}e^{-\sqrt{E_G/E}}$.
- Gamow peak: $E_0 = [E_G(k_BT)^2/4]^{1/3}$, $\Delta = 4\sqrt{E_0 k_B T/3}$.
- D + T is the most accessible laboratory fuel cycle, aided by broad resonant nuclear structure; triple-alpha is a sequential resonant process outside the binary formula.

1.7 Deeper physics: Gamow peak, $\langle\sigma v\rangle$, and stellar rates

1.7.1 Thermal average and the Gamow peak

In a plasma at temperature T, the fusion rate per unit volume for species X and Y is $r = n_X n_Y \langle\sigma v\rangle$, where

$$\langle\sigma v\rangle = \int_0^\infty \sigma(v)\, v\, f(v)\, \mathrm{d}v \tag{1.37}$$

and $f(v)$ is the Maxwell–Boltzmann distribution of relative speeds at temperature T [14, 6]. At low energy, $\sigma(E) \propto E^{-1}e^{-b/\sqrt{E}}$ (Gamow factor), so the integrand $\sigma v f(v)$ peaks at a finite energy E_0 well below the Coulomb barrier. This **Gamow peak** is where most stellar fusion occurs: neither the mean thermal energy k_BT nor the barrier height alone sets the rate [36, 2].

Gamow peak for $p + p$ at solar core temperature

At $T = 15 \times 10^6\,\mathrm{K}$, $k_BT \approx 1.3\,\mathrm{keV}$. For $p + p$ fusion, the Gamow peak sits near $E_0 \sim 6$–$7\,\mathrm{keV}$, roughly five times k_BT [14, 36]. The cross section at E_0 is extraordinarily small ($\sim 10^{-47}\,\mathrm{cm}^2$), yet the solar core density ($\sim 150\,\mathrm{g\,cm^{-3}}$) and long confinement time yield a stable $4 \times 10^{26}\,\mathrm{W}$ luminosity. The weak $p + p$ step sets the overall timescale [6, 36].

1.7.2 The S-factor and practical rate formula

Laboratory data are quoted as the astrophysical S-factor,

$$\sigma(E) = \frac{S(E)}{E}\exp\left(-\sqrt{\frac{E_G}{E}}\right), \qquad E_G = 2\mu(\pi\alpha Z_1 Z_2 \hbar c)^2, \tag{1.38}$$

which removes the steep Gamow energy dependence [14, 36]. Near the Gamow peak, a useful approximation is

$$\langle\sigma v\rangle \approx \sqrt{\frac{8}{3\pi}}\,\frac{S(E_0)}{E_0^2}\,(k_BT)^{3/2}\,\exp(-3E_0/k_BT)\,, \tag{1.39}$$

showing the strong T dependence that makes CNO burning dominate in more massive stars [6, 1]. Recommended $S(E)$ values and uncertainties are maintained in Solar Fusion III [36].

Key idea

Closing the arc: decay, reactions, fission, fusion. The Gamow exponent first appeared in α decay (Lectures 16–17), reappears as fusion tunneling (Lecture 25), and sets stellar lifetimes through $\langle\sigma v\rangle$. Fission and fusion bracket the binding-energy curve: heavy nuclei split, light nuclei merge, both releasing Q when the products are more tightly bound

[6, 14, 2].

1.7.3 Resonances and the Hoyle state

When a narrow resonance sits in the Gamow window, the thermal average is dominated by the Breit–Wigner contribution [14, 6]. The Hoyle state in ^{12}C at $E_r \approx 7.65\,\mathrm{MeV}$ makes the 3α process possible in red giants: without it, carbon would not form in stars [2, 14]. The resonance contribution adds to, not replaces, the non-resonant $\langle\sigma v\rangle$ of (1.37). Screening in stellar plasmas enhances all channels by $f_{\mathrm{sc}} \approx \exp(U_e/k_BT)$ with $U_e \sim 1$–$2\,\mathrm{keV}$ at solar core conditions [36, 14].

1.7.4 CNO cycle temperature sensitivity

The CNO-I loop regenerates ^{12}C and converts four protons to ^{4}He with the same net energy release as the *pp* chain [1, 36]. Because CNO reactions involve higher Z projectiles, their Coulomb barriers are higher and $\langle\sigma v\rangle$ is more temperature sensitive ($\sim T^{15}$ to T^{20} near main-sequence temperatures) than the *pp* chain ($\sim T^4$) [36, 6]. Massive stars with $T_{\mathrm{core}} \gtrsim 1.7\times10^7\,\mathrm{K}$ therefore switch to CNO-dominated energy generation. Precision S-factors for $^{14}\mathrm{N}(p,\gamma)^{15}\mathrm{O}$ and related branches remain active research topics because solar and stellar models propagate their uncertainties into age and metallicity determinations [36, 51].

Screening corrections in laboratory targets enhance low-energy fusion relative to bare-nucleus S-factors; stellar plasma screening differs again. When comparing a measured low-energy cross section to Solar Fusion III recommendations, check whether screening was unfolded. Electron screening is a systematic, not a curiosity, at Gamow-window energies.

1.8 Further physics from the literature

Astrophysical S-factor. Writing $\sigma(E) = S(E)E^{-1}e^{-b/\sqrt{E}}$ removes the dominant Coulomb energy dependence so that $S(E)$ is nearly constant or slowly varying. Extrapolating $S(E)$ from laboratory energies (hundreds of keV) down to the Gamow window (tens of keV in the Sun) is a central task of nuclear astrophysics [14, 6, 36].

The solar *pp* chain. The initiating weak reaction and rapid deuterium capture are

$$p + p \to d + e^+ + \nu_e, \qquad Q_{\mathrm{nuc}} = 0.420\,\mathrm{MeV}, \tag{1.40}$$

$$d + p \to {}^3\mathrm{He} + \gamma, \qquad Q = 5.493\,\mathrm{MeV}. \tag{1.41}$$

The dominant *pp*-I termination is $^3\mathrm{He} + {}^3\mathrm{He} \to {}^4\mathrm{He} + 2p$; the *pp*-II and *pp*-III branches proceed through ^{7}Be, with ^{8}B beta decay producing the highest-energy solar neutrinos. All branches have the same net nuclear bookkeeping,

$$4p \to {}^4\mathrm{He} + 2e^+ + 2\nu_e, \tag{1.42}$$

followed by positron annihilation in matter [6, 1, 36].

CNO catalysis. In the main CNO-I loop,

$$^{12}\mathrm{C}(p,\gamma)^{13}\mathrm{N}(\beta^+\nu_e)^{13}\mathrm{C}(p,\gamma)^{14}\mathrm{N}(p,\gamma)^{15}\mathrm{O}(\beta^+\nu_e)^{15}\mathrm{N}(p,\alpha)^{12}\mathrm{C}.$$

The ^{12}C catalyst is regenerated, so the net reaction is again four protons to one alpha plus two positrons and two neutrinos. Its stronger temperature sensitivity makes CNO burning increasingly important in hotter, more massive main-sequence stars; in the Sun it is subdominant [1, 36].

Neutrino energy accounting. Using neutral-atom masses, the complete conversion $4\,^1\mathrm{H} \to {}^4\mathrm{He}$ releases $Q = 26.73\,\mathrm{MeV}$. This is the nuclear energy release, not all of the heat deposited in the star. Neutrinos escape with branch-dependent energies, so

$$Q_{\text{heat}} = 26.73\,\mathrm{MeV} - \sum_{\nu}\langle E_\nu\rangle. \tag{1.43}$$

Positron annihilation energy is already accounted for consistently when atomic masses are used; adding it a second time would double count it [36].

Resonances. When a compound nuclear level sits in the Gamow window, $\sigma(E)$ can be resonantly enhanced (Breit–Wigner). The 3α process that forms carbon in red giants is a classic example (Hoyle state in ^{12}C) [14, 2]. For an isolated narrow resonance at E_r, the Maxwellian average scales as

$$\langle\sigma v\rangle_r = \left(\frac{2\pi}{\mu k_B T}\right)^{3/2}\hbar^2(\omega\gamma)e^{-E_r/k_BT}, \tag{1.44}$$

where $\omega\gamma$ is the resonance strength. This contribution must be added to, not hidden inside, the slowly varying nonresonant approximation.

Screening. For weak static screening with screening energy $U_e \ll E_0$, a useful local estimate is $f_{\text{sc}} \simeq \exp(U_e/k_BT)$, so that the bare-nucleus rate is multiplied by f_{sc}. Strongly coupled plasmas and laboratory electron-screening corrections require more careful treatments [14, 36].

Lawson criterion and ignition. A crude balance of fusion power against losses leads to a minimum $n\tau_E$ (or $nT\tau_E$) for net energy gain. Different fuel cycles and confinement schemes shift the required temperature and the peak of $\langle\sigma v\rangle$ [1, 6].

Neutron budgets in D + T. The 14 MeV neutron must be moderated and captured (often on lithium) to breed tritium if a closed fuel cycle is desired. Neutron damage to structural materials is a major engineering challenge [1, 2].

Reading guide

Basdevant [14] (Gamow peak and stellar rates); Krane [6] (cross sections and reactors); Dunlap [1] (plasma fusion concepts); Demtröder [2] (broader survey); Verma [32] (Nuclear Fusion Parts 1–2 and stellar neutrinos); Solar Fusion III [36] for recommended S-factors.

Nuclear data for light-ion reactions: evaluated libraries and ENSDF/NuDat for residual nuclei [20, 21].

1.8.1 Locating the Gamow peak analytically

For $\sigma(E) \propto E^{-1}\exp(-\sqrt{E_G/E})$ and a Maxwellian weight $E^{1/2}\exp(-E/k_BT)$, the integrand in (1.37) peaks where

$$\frac{\mathrm{d}}{\mathrm{d}E}\left[E^{-1/2}\exp\left(-\sqrt{\frac{E_G}{E}}-\frac{E}{k_BT}\right)\right]=0. \tag{1.45}$$

The approximate solution is $E_0 \approx (E_G(k_BT)^2/4)^{1/3}$, the Gamow peak energy [14, 6]. The width of the peak is roughly $\Delta E \sim 4\sqrt{E_0k_BT/3}$. Reactions are sensitive to $S(E)$ evaluated at E_0, not at the mean thermal energy [36, 2].

Solar $p+p$ rate order of magnitude

With $S_{pp}(0) \approx 4\times10^{-25}\,\mathrm{MeV\,b}$ from Solar Fusion III, $E_G \approx 493\,\mathrm{keV}$ for $p+p$, and $T = 15\times10^6\,\mathrm{K}$, the practical formula (1.39) gives $\langle\sigma v\rangle_{pp} \sim 10^{-47}\,\mathrm{cm^3\,s^{-1}}$ [36, 14]. At $\rho \approx 150\,\mathrm{g\,cm^{-3}}$ and $X_p \approx 0.35$, the proton density is $n_p \sim 10^{26}\,\mathrm{cm^{-3}}$, so the local *pp* rate per unit volume is $\sim 10^{-21}\,\mathrm{cm^{-3}\,s^{-1}}$. Integrated over the solar core volume this sustains the observed luminosity [6, 36].

1.8.2 Closing the course arc: decay, reactions, fission, fusion

The Gamow exponent entered as α-decay tunneling (Lectures 16–17), reappeared in sub-barrier fusion (Lecture 25), and sets stellar lifetimes through $\langle\sigma v\rangle$. Weak β decay (Lectures 18–19) limits the *pp* chain rate. Multipole γ de-excitation (Lecture 20) follows reaction and decay cascades. Direct and compound reactions (Lecture 21) and two-body kinematics (Lecture 22) connect laboratory measurements to astrophysical networks. Fission (Lectures 23–24) terminates the heavy-nucleus stability region; fusion builds light nuclei up the binding curve. All share Q-value bookkeeping from the SEMF and mass tables [6, 27, 14].

Key idea

Temperature sensitivity. CNO burning scales roughly as $\langle\sigma v\rangle \propto T^{15}$ to T^{20} near main-sequence temperatures, far steeper than the *pp* chain $\propto T^4$ [36, 1]. This strong temperature dependence explains why massive stars switch to CNO-dominated cores and why terrestrial fusion devices must hold $T \sim 10^8\,\mathrm{K}$ for D–T ignition [6, 2].

1.8.3 Neutrino flux and the weak steps in the *pp* chain

The *pp* chain releases $Q = 26.73\,\mathrm{MeV}$ per $4\,{}^1\mathrm{H}$ to ${}^4\mathrm{He}$, but neutrinos carry 2–25% of that energy depending on the branch [36, 6]. The initiating $p+p\to d+e^++\nu_e$ step is weak (Lecture 18) and therefore slow; the subsequent strong captures proceed quickly once deuterium forms. Solar neutrino experiments test both the nuclear S-factors and the weak-interaction rate [36, 2].

Recommended rates and uncertainties in Solar Fusion III propagate directly into helioseismology and solar-age determinations [36, 14].

1.8.4 Lawson criterion and the D–T fuel choice

The Lawson product $n\tau_E$ required for net energy gain depends on $\langle\sigma v\rangle(T)$ and on loss mechanisms in the confinement scheme [1, 6]. D–T is chosen for terrestrial devices because $\langle\sigma v\rangle$ peaks at accessible temperatures near 10^8 K, not because it has the lowest Coulomb barrier among all fuel cycles [2]. The *pp* chain in the Sun trades a lower Coulomb barrier for a weak-interaction bottleneck (Lecture 18), producing a stable gigayear burn rate [36, 14]. Reading Solar Fusion III tables with the Gamow-peak map from this lecture identifies which S-factors are experimentally anchored near stellar energies and which still rely on extrapolation [36, 52].

1.9 Deeper reading: stellar rates and the Gamow window

The reaction rate $\langle\sigma v\rangle$ weights the Maxwell–Boltzmann tail against tunneling through the Coulomb barrier. The Gamow peak energy is where that product maximises; most stellar burning occurs near that window, not at the Gamow energy of a single particle with mean thermal energy. Solar Fusion III tabulates recommended S-factors and uncertainties for *pp*-chain and CNO reactions.

A 10% change in a well-measured S-factor is not equivalent to a 10% change in an extrapolated one: neutrino-flux sensitivities make the distinction quantitative. Underground accelerators push laboratory energies toward the Gamow window. Link back to Lecture 25's barrier and to Lecture 6's stellar endpoints: nuclear rates are the microphysics inside the macroscopic stellar structure.

S-factor definition

Writing $\sigma(E) = S(E)E^{-1}e^{-2\pi\eta}$ removes most of the Coulomb exponential so that $S(E)$ varies slowly and can be extrapolated. Always state whether $S(0)$ or $S(E_0)$ at the Gamow peak is quoted. Polynomial or R-matrix extrapolations encode different nuclear-structure assumptions.

Neutrino diagnostics

Solar neutrino fluxes depend on core temperature and on specific nuclear rates. A change in $^7\mathrm{Be}(p,\gamma)^8\mathrm{B}$ moves the high-energy neutrino flux almost linearly, whereas *pp* rate changes are partly compensated by stellar-structure feedback. Sensitivity studies in Solar Fusion III make that hierarchy explicit for students who only met $\langle\sigma v\rangle$ algebra in this chapter.

Gamow-peak numerics

For $p+p$ at $T = 15\times10^6$ K, estimate kT, the Gamow energy, and the width of the Gamow window using textbook formulas. Compare kT with the Gamow peak energy: they differ substantially, which is the whole point of the peak construction. Then open Solar Fusion III tables and record $S(0)$ and uncertainty for $^7\mathrm{Be}(p,\gamma)^8\mathrm{B}$ and for a CNO reaction.

Discuss how a 5% rate change propagates differently into *pp* and ^{8}B neutrino fluxes because of stellar-structure feedback. This sensitivity language turns the Lecture 26 algebra into the reason underground accelerators and solar-neutrino experiments are a single scientific programme.

The Gamow peak is why stars burn at energies far below the Coulomb barrier. Solar Fusion III turns that idea into recommended S-factors and neutrino-aware uncertainties.

In practice, rework one numerical estimate from the lecture with a different parameter set and compare the shift to the quoted experimental uncertainty. If the shift exceeds the uncertainty, the estimate is teaching a scale, not delivering a fit. That distinction keeps theoretical cartoons honest when they sit beside evaluated data tables and modern many-body calculations. Along the course arc, write one sentence linking this chapter backward and one forward: the discipline of those two sentences is as important as any single formula. Examination problems rarely ask for a literature review, but they do ask for the scale argument that literature reviews presuppose.

Synthesis problem

Write a half-page note that (i) restates the chapter's central scale or selection rule in one equation, (ii) evaluates it numerically for one concrete nucleus or energy, and (iii) names the neighbouring lecture that uses the result. Keep the note free of research-frontier speculation; the goal is fluency with the lecture physics itself. If an assumption fails (Born approximation, spherical mean field, allowed transition, one-dimensional barrier), state the failure mode in a final sentence. That habit converts passive reading into examination-ready understanding and makes the later research-frontier box read as an extension rather than a replacement.

Research frontier: stellar rates, neutrinos, and Solar Fusion III

The Gamow-peak rate $\langle \sigma v \rangle$ of Lecture 26 is the quantitative bridge from laboratory cross sections to stellar models. Solar Fusion III provides recommended S-factors and uncertainties for *pp*-chain and CNO reactions, driven by few-percent solar-neutrino measurements and by underground accelerator data that push closer to stellar energies [36]. The same nuclear inputs feed models of Population II stars, classical novae, and the early stages of massive-star evolution, while multimessenger astrophysics adds complementary constraints from compact-object mergers [46, 52]. Remaining uncertainties include several subdominant CNO and *pp*-chain S-factors, electron-screening corrections at stellar energies, and the propagation of nuclear-rate covariances into neutrino-flux predictions. Underground laboratories continue to reduce those errors by measuring closer to the Gamow window. The lecture's analytic Gamow peak therefore remains the conceptual map for reading Solar Fusion III tables.

When reading Solar Fusion III, students should note which S-factors are limited by experiment near the Gamow window and which still rely on extrapolation or theory. A 10% change in a well-measured rate is not equivalent to a 10% change in a sparsely constrained one; neutrino-flux sensitivities make that distinction quantitative.

Not every 10% S-factor change is equal: neutrino-flux sensitivities weight well-measured and extrapolated rates differently.

Student directions. (1) Numerical exercise: locate the Gamow peak for $p+p$ at $T = 15\times10^6$ K. (2) Table lookup: using Solar Fusion III, quote the recommended $S(0)$ and uncertainty for

^{7}Be$(p,\gamma)^8$B. (3) Sensitivity discussion: explain how a 10% change in one CNO S-factor propagates into the solar core temperature inferred from neutrinos.

1.10 Problems with solutions

Problem 26.1 — Derive $R = n_X n_Y \sigma v$

A beam of Y nuclei with density n_Y and speed v strikes a medium with target density n_X. Using the cylinder of area σ and length $v\,dt$, derive the volumetric reaction rate R. Then state the thermal-plasma result for unlike species and for identical reactants [6, 14].

Solution 26.1

Step 1. Volume swept relative to one X in time dt: $\sigma v\,dt$.

Step 2. Number of Y in that volume: $n_Y \sigma v\,dt$. Rate per X: $\lambda = n_Y \sigma v$.

Step 3. Per unit volume there are n_X targets, so

$$R = n_X n_Y \sigma v.$$

In a plasma, average over relative velocities. For unlike species,

$$R_{XY} = n_X n_Y \langle \sigma v \rangle.$$

For identical reactants, unordered-pair counting supplies the required factor:

$$R_{XX} = \frac{1}{2} n_X^2 \langle \sigma v \rangle.$$

Problem 26.2 — Annular partial-wave area

Show that the area between impact parameters $b_\ell = \ell\hbar/(\mu v)$ and $b_{\ell+1}$ equals $\pi\hbar^2(2\ell+1)/(\mu^2 v^2)$. Explain why this $1/v^2$ partial-wave prefactor does *not* by itself imply that a charged-particle fusion cross section grows as $1/v^2$ at low energy.

Solution 26.2

Step 1.

$$A_\ell = \pi\Big(\frac{(\ell+1)\hbar}{\mu v}\Big)^2 - \pi\Big(\frac{\ell\hbar}{\mu v}\Big)^2 = \frac{\pi\hbar^2}{\mu^2 v^2}\left[(\ell+1)^2 - \ell^2\right] = \frac{\pi\hbar^2}{\mu^2 v^2}(2\ell+1).$$

Step 2. Summing $\ell = 0 \ldots \ell_{\max}$ with $\ell_{\max} \sim \mu v R/\hbar$ gives $\sigma \sim \pi(R + \hbar/(\mu v))^2$. If $\hbar/(\mu v) \gg R$, $\pi\hbar^2/(\mu^2 v^2)$ is the entrance-channel area scale. The reaction probability also contains the transmission coefficient. For a nonresonant charged-particle reaction, $\sigma(E) = S(E) E^{-1} e^{-\sqrt{E_G/E}}$, so Coulomb suppression dominates as $E \to 0$ [14, 6].

Problem 26.3 — Gamow exponent with units

Starting from $\eta = Z_1 Z_2 \alpha c/v$ and $E = \frac{1}{2}\mu v^2$, derive $2\pi\eta = \sqrt{E_G/E}$ and $E_G = 2\mu c^2(\pi\alpha Z_1 Z_2)^2$. Check the dimensions.

Solution 26.3

Step 1. $v = \sqrt{2E/\mu}$, so

$$2\pi\eta = 2\pi Z_1 Z_2 \alpha c \sqrt{\frac{\mu}{2E}} = \sqrt{\frac{2\mu c^2(\pi\alpha Z_1 Z_2)^2}{E}}.$$

Step 2. Identifying the numerator as E_G gives $2\pi\eta = \sqrt{E_G/E}$. Since μc^2 is an energy and π, α, Z_1, Z_2 are dimensionless, E_G has energy units.

Step 3. Larger $Z_1 Z_2$ raises $E_G \propto Z_1^2 Z_2^2$, making $P \propto e^{-\sqrt{E_G/E}}$ exponentially smaller. Heavy-ion fusion at thermonuclear energies is vastly harder than hydrogen fusion [6, 1].

Problem 26.4 — Gamow peak and width

Starting from $I(E) = \exp[-E/(k_B T) - \sqrt{E_G/E}]$, derive E_0 and the full $1/e$ width Δ. Evaluate both for $p + p$ at $T = 1.5 \times 10^7$ K, using $E_G = 489\,\text{keV}$ and $k_B T = 1.293\,\text{keV}$.

Solution 26.4

Step 1. Minimise $\Phi(E) = E/(k_B T) + \sqrt{E_G} E^{-1/2}$:

$$\frac{\mathrm{d}\Phi}{\mathrm{d}E} = \frac{1}{k_B T} - \frac{\sqrt{E_G}}{2} E^{-3/2} = 0.$$

Step 2.

$$E_0 = \left[\frac{E_G (k_B T)^2}{4}\right]^{1/3} = \left[\frac{(489)(1.293)^2}{4}\right]^{1/3} = 5.89\,\text{keV}.$$

Step 3. Since $\Phi''(E_0) = 3/(2E_0 k_B T)$,

$$\Phi(E) \simeq \Phi(E_0) + \frac{3(E - E_0)^2}{4E_0 k_B T}.$$

At the $1/e$ points $E - E_0 = \pm\Delta/2$, hence

$$\Delta = 4\sqrt{\frac{E_0 k_B T}{3}} = 4\sqrt{\frac{(5.89)(1.293)}{3}} = 6.38\,\text{keV}.$$

The reacting window is well above $k_B T$ but far below the contact barrier [14, 36].

Problem 26.5 — Rate scaling with density

A plasma of identical fuel nuclei has density n and reactivity $\langle\sigma v\rangle$. Write R including the identical-particle factor $\frac{1}{2}$. If n is doubled at fixed T, by what factor does R change?

Solution 26.5

$$R = \frac{1}{2}n^2\langle\sigma v\rangle.$$

Doubling n multiplies R by 4. Fusion power density is quadratic in density at fixed temperature [6, 1].

Problem 26.6 — D + T energetics

In $\mathrm{D}+\mathrm{T} \to {}^4\mathrm{He}+n+17.6\,\mathrm{MeV}$, the α and neutron share momentum. Show that the neutron carries about 14.1 MeV and the α about 3.5 MeV (nonrelativistic two-body kinematics in the CM frame).

Solution 26.6

Step 1. In the CM frame, $p_\alpha = p_n = p$ and

$$\frac{p^2}{2m_\alpha} + \frac{p^2}{2m_n} = Q.$$

Step 2. With $m_\alpha \approx 4m_n$,

$$K_n = \frac{m_\alpha}{m_\alpha + m_n}Q = \frac{4}{5}Q = 0.8 \times 17.6 = 14.08\,\mathrm{MeV},$$

$$K_\alpha = \frac{m_n}{m_\alpha + m_n}Q = \frac{1}{5}Q = 3.52\,\mathrm{MeV}.$$

The neutron carries $\sim 80\%$ of Q; in magnetic fusion it escapes the confining field and heats a blanket, while the charged α can heat the plasma [6, 14].

Bibliography

[1] R. A. Dunlap, *An Introduction to the Physics of Nuclei and Particles* (2nd ed.), IOP Publishing, Bristol (2023), DOI: 10.1088/978-0-7503-6094-4, Ch. 3 (Nuclear composition and size).

[2] W. Demtröder, *Nuclear and Particle Physics*, Undergraduate Lecture Notes in Physics, Springer, Cham (2023).

[3] S. Petrera, *Problems and Solutions in Nuclear and Particle Physics*, UNITEXT for Physics, Springer, Cham (2019).

[4] F. Terranova, *A Modern Primer in Particle and Nuclear Physics*, Oxford University Press (2021).

[5] S. D'Auria, *Introduction to Nuclear and Particle Physics*, Undergraduate Lecture Notes in Physics, Springer, Cham (2018).

[6] K. S. Krane, *Introductory Nuclear Physics*, Wiley, New York (1988).

[7] R. Hofstadter, "Electron scattering and nuclear structure," Rev. Mod. Phys. **28**, 214 (1956).

[8] H. F. Ehrenberg, R. Hofstadter, U. Meyer-Berkhout, D. G. Ravenhall, and S. E. Sobottka, "High-Energy Electron Scattering and the Charge Distribution of Carbon-12 and Oxygen-16," Phys. Rev. **113**, 666 (1959).

[9] H. Yukawa, "On the interaction of elementary particles. I," Proc. Phys.-Math. Soc. Japan **17**, 48 (1935).

[10] R. D. Woods and D. S. Saxon, "Diffuse surface optical model for nucleon-nuclei scattering," Phys. Rev. **95**, 577 (1954).

[11] H. G. J. Moseley, "The high-frequency spectra of the elements," Phil. Mag. **26**, 1024 (1913); **27**, 703 (1914).

[12] C. F. von Weizsäcker, "Zur Theorie der Kernmassen," Z. Phys. **96**, 431 (1935).

[13] P. Cappellaro, *Introduction to Applied Nuclear Physics* (MIT OpenCourseWare / LibreTexts), CC BY-NC-SA 4.0.

[14] J.-L. Basdevant, J. Rich, and M. Spiro, *Fundamentals in Nuclear Physics: From Nuclear Structure to Cosmology*, Springer, New York (2005).

[15] D. Tong, *Particle Physics*, Lecture notes (University of Cambridge / CERN school notes).

[16] M. G. Mayer, "On closed shells in nuclei. II," Phys. Rev. **75**, 1969 (1949).

[17] O. Haxel, J. H. D. Jensen, and H. E. Suess, "On the "magic numbers" in nuclear structure," Phys. Rev. **75**, 1766 (1949).

[18] T. Schmidt, "Über die magnetischen Momente der Atomkerne," Z. Phys. **106**, 358 (1937).

[19] L. W. Nordheim, "On spins, moments, and shells in nuclei," Phys. Rev. **78**, 294 (1950).

[20] Evaluated Nuclear Structure Data File (ENSDF), National Nuclear Data Center, Brookhaven National Laboratory, `https://www.nndc.bnl.gov/ensdf/`.

[21] NuDat 3, National Nuclear Data Center, Brookhaven National Laboratory, `https://www.nndc.bnl.gov/nudat3/`.

[22] N. J. Stone, "Table of nuclear magnetic dipole and electric quadrupole moments," At. Data Nucl. Data Tables **90**, 75 (2005); updated compilations at NNDC.

[23] W. N. Cottingham and D. A. Greenwood, *An Introduction to Nuclear Physics* (2nd ed.), Cambridge University Press, Cambridge (2001).

[24] H. Geiger and J. M. Nuttall, "The ranges of the α particles from the radioactive substances," Phil. Mag. **22**, 613 (1911).

[25] G. Gamow, "Zur Quantentheorie des Atomkernes," Z. Phys. **51**, 204 (1928).

[26] R. W. Gurney and E. U. Condon, "Wave mechanics and radioactive disintegration," Nature **122**, 439 (1928); Phys. Rev. **33**, 127 (1929).

[27] M. Wang, W. J. Huang, F. G. Kondev, G. Audi, and S. Naimi, "The AME 2020 atomic mass evaluation (II). Tables, graphs and references," Chin. Phys. C **45**, 030003 (2021).

[28] Laboratoire National Henri Becquerel (LNHB), Recommended decay data, `http://www.lnhb.fr/nuclear-data/nuclear-data-table/`.

[29] L. M. Langer, R. D. Moffat, and H. C. Price, Jr., "Low energy beta-ray spectra: P^{32} and Cu^{64}," Phys. Rev. **76**, 1725 (1949).

[30] L. M. Langer and H. C. Price, Jr., "Shapes of the beta-spectra of the forbidden transitions of Sb^{124}, Rb^{86}, Sr^{89}, Y^{91}, and Cs^{137}," Phys. Rev. **75**, 1769 (1949).

[31] D. C. Camp and L. M. Langer, "The shape of the ^{66}Ga positron spectrum and the contribution from $0^+ \to 0^+$ transitions," Phys. Rev. **129**, 1782 (1963).

[32] H. C. Verma, *Nuclear Physics: Fundamentals and Applications*, NPTEL/IIT Kanpur lecture series, `https://hcverma.in/ncl_phy_lectures`.

[33] International Atomic Energy Agency, *LiveChart of Nuclides*, evaluated structure, decay, reaction, and fission-yield data, `https://www-nds.iaea.org/relnsd/vcharthtml/VChartHTML.html`.

[34] T. Kibédi, T. W. Burrows, M. B. Trzhaskovskaya, P. M. Davidson, and C. W. Nestor, Jr., "Evaluation of theoretical conversion coefficients using BrIcc," Nucl. Instrum. Methods Phys. Res. A **589**, 202 (2008), DOI: 10.1016/j.nima.2008.02.051.

[35] D. A. Brown *et al.*, "ENDF/B-VIII.0: The 8th major release of the nuclear reaction data library with CIELO-project cross sections, new standards and thermal scattering data," Nucl. Data Sheets **148**, 1 (2018), DOI: 10.1016/j.nds.2018.02.001.

[36] B. Acharya *et al.*, "Solar fusion III: New data and theory for hydrogen-burning stars," Rev. Mod. Phys. **97**, 035002 (2025), DOI: 10.1103/8lm7-gs18.

[37] S. N. Ghoshal, "An experimental verification of the theory of compound nucleus," Phys. Rev. **80**, 939 (1950), DOI: 10.1103/PhysRev.80.939.

[38] D. Adhikari *et al.* (PREX Collaboration), "Accurate determination of the neutron skin thickness of ^{208}Pb through parity-violation in electron scattering," Phys. Rev. Lett. **126**, 172502 (2021), DOI: 10.1103/PhysRevLett.126.172502.

[39] B. T. Reed, F. J. Fattoyev, C. J. Horowitz, and J. Piekarewicz, "Implications of PREX-II on the equation of state of neutron-rich matter," Phys. Rev. Lett. **126**, 172503 (2021), DOI: 10.1103/PhysRevLett.126.172503.

[40] B. Hu *et al.*, "Ab initio predictions link the neutron skin of ^{208}Pb to nuclear forces," Nature Phys. **18**, 1196 (2022), DOI: 10.1038/s41567-022-01715-8.

[41] E. Epelbaum, H.-W. Hammer, and U.-G. Meißner, "Modern theory of nuclear forces," Rev. Mod. Phys. **81**, 1773 (2009), DOI: 10.1103/RevModPhys.81.1773.

[42] H.-W. Hammer, S. König, and U. van Kolck, "Nuclear effective field theory: Status and perspectives," Rev. Mod. Phys. **92**, 025004 (2020), DOI: 10.1103/RevModPhys.92.025004.

[43] T. Otsuka, A. Gade, O. Sorlin, T. Suzuki, and Y. Utsuno, "Evolution of shell structure in exotic nuclei," Rev. Mod. Phys. **92**, 015002 (2020), DOI: 10.1103/RevModPhys.92.015002.

[44] H. Hergert, S. K. Bogner, T. D. Morris, A. Schwenk, and K. Tsukiyama, "The in-medium similarity renormalization group: A novel ab initio method for nuclei," Phys. Rep. **621**, 165 (2016), DOI: 10.1016/j.physrep.2015.12.007.

[45] J. M. Lattimer and M. Prakash, "The equation of state of hot, dense matter and neutron stars," Phys. Rep. **621**, 127 (2016), DOI: 10.1016/j.physrep.2015.12.005.

[46] J. M. Lattimer, "Neutron stars and the nuclear matter equation of state," Annu. Rev. Nucl. Part. Sci. **71**, 433 (2021), DOI: 10.1146/annurev-nucl-102419-124827.

[47] B. P. Abbott *et al.* (LIGO Scientific Collaboration and Virgo Collaboration), "GW170817: Observation of gravitational waves from a binary neutron star inspiral," Phys. Rev. Lett. **119**, 161101 (2017), DOI: 10.1103/PhysRevLett.119.161101.

[48] M. J. Dolinski, A. W. P. Poon, and W. Rodejohann, "Neutrinoless double-beta decay: Status and prospects," Annu. Rev. Nucl. Part. Sci. **69**, 219 (2019), DOI: 10.1146/annurev-nucl-101918-023407.

[49] M. Agostini, G. Benato, J. A. Detwiler, J. Menéndez, and F. Vissani, "Toward the discovery of matter creation with neutrinoless $\beta\beta$ decay," Rev. Mod. Phys. **95**, 025002 (2023), DOI: 10.1103/RevModPhys.95.025002.

[50] P. Gysbers *et al.*, "Discrepancy between experimental and theoretical β-decay rates resolved from first principles," Nature Phys. **15**, 428 (2019), DOI: 10.1038/s41567-019-0450-7.

[51] H. L. Crawford, K. Fossez, S. König, and A. Spyrou, "A vision for the science of rare isotopes," Annu. Rev. Nucl. Part. Sci. **74**, 141 (2024), DOI: 10.1146/annurev-nucl-121423-091501.

[52] Nuclear Science Advisory Committee, *A New Era of Discovery: The 2023 Long Range Plan for Nuclear Science*, U.S. Department of Energy and National Science Foundation (2023), `https://nuclearsciencefuture.org/`.

[53] S. A. Giuliani, Z. Matheson, W. Nazarewicz, E. Olsen, P.-G. Reinhard, J. Sadhukhan, B. Schuetrumpf, N. Schunck, and P. Schwerdtfeger, "Colloquium: Superheavy elements: Oganesson and beyond," Rev. Mod. Phys. **91**, 011001 (2019), DOI: 10.1103/RevModPhys.91.011001.

[54] N. Schunck and D. Regnier, "Theory of nuclear fission," Prog. Part. Nucl. Phys. **125**, 103963 (2022), DOI: 10.1016/j.ppnp.2022.103963.

[55] I. Counts, J. Hur, D. P. L. Aude Craik, H. Jeon, C. Leung, J. C. Berengut, A. Geddes, A. Kawasaki, W. Jhe, and V. Vuletić, "Evidence for nonlinear isotope shift in Yb^+ search for new boson," Phys. Rev. Lett. **125**, 123002 (2020), DOI: 10.1103/PhysRevLett.125.123002.

[56] I. Angeli and K. P. Marinova, "Table of experimental nuclear ground state charge radii: An update," At. Data Nucl. Data Tables **99**, 69 (2013), DOI: 10.1016/j.adt.2011.12.006.

[57] S. Kraemer *et al.*, "Observation of the radiative decay of the ^{229}Th nuclear clock isomer," Nature **617**, 706 (2023), DOI: 10.1038/s41586-023-05894-z.